Int. J. Electrochem. Sci., 12 **(2017)** 9378 – 9397, doi: 10.20964/2017.10.31

International Journal of
ELECTROCHEMICAL
SCIENCE
www.electrochemsci.org

Electrochemical Characterization of Nickel in Oxalic Acid Solutions and the Effect of Halides and Azide Ions Additions on Its Behavior

F. El-Taib Heakal[1,*], *O.S. Shehata*[2], *N.S. Tantawy*[3]

[1] Chemistry Department, Faculty of Science, Cairo University, Giza 12613, Egypt.
[2] Physical Chemistry Department, National Research Centre, Dokki, Giza 12622, Egypt.
[3] Faculty of Women for Arts, Science and Education, Ain Shams University, Cairo, Egypt.
[*]E-mail: fakihaheakal@yahoo.com, feltaibheakal@gmail.com

Received: 9 May 2017 / *Accepted:* 19 July 2017 / *Published:* 12 September 2017

The electrochemical behavior of polycrystalline nickel in aqueous oxalic acid solutions was thoroughly investigated using different electrochemical techniques. Open circuit potential (OCP) transients of Ni electrode indicate different natural tendencies for the metal to modify its pre-immersion native film in oxalic acid medium depending on its concentration and temperature. In agreement with the OCP results, electrochemical impedance spectroscopy (EIS) clearly demonstrates that surface film resistance (R_f) on Ni increases with concentration over the range 0.01-0.5 M, but decreases with raising temperature. Also, linear sweep voltammetry (LSV) was used to compare at similar experimental conditions hydrogen evolution reaction (HER) on nickel cathode to that on platinum which has high catalytic activity towards HER. Furthermore, addition of different sodium halides or azide to 0.5 M oxalic acid solution (blank) was found to increase the propensity of nickel to dissolution in the following order: $I^- < F^- <$ blank acid $< Cl^- < Br^- < N_3^-$ (the most aggressive). These findings are discussed based on the kosmotrope/chaotrope nature of the added anions and further validated by SEM examination.

Keywords: Nickel metal; Oxalic acid; Halides; Azide ions; EIS; LSV; SEM; Film resistance.

1. INTRODUCTION

The recognized electrocatalytic properties and stability of polycrystalline nickel has much attracted attention on increasing its widespread applications in many industrial sectors [1-8]. Indeed, nickel can be considered a slightly noble metal, as its domain of thermodynamic stability has a small zone in common with that of water. Accordingly, the corrosion resistance of nickel should depend on

the pH and the presence of oxidizing agent for non-completing solutions [9]. The excellent corrosion resistance of nickel and nickel-based materials are attributed to formation of passive films on their surfaces, mainly composed of oxides that are extremely thin ~1 nm [10]. The nature of those passive films and their mechanisms depend on other factors such as electrolyte nature and concentration [11,12], and on the metal structure modification [13,14].

To date, ample reports in the literature have been published regarding the electrochemical behavior of nickel and the mechanism of its passive film formation in several inorganic acid solutions [14-23]. Nevertheless, there are few studies that are insufficient to allow enough information in organic acids despite the importance of those acids and their extensive usage in the industrial synthesis and processing of metallic surfaces [24-28]. Therefore, the present study was undertaken in order to gain new information that might be of importance in many fields. Among the various organic acids, oxalic acid $(COOH)_2$ is of increasing importance as it is relatively strong in its first stage of dissociation due to the proximity of the second carboxylic group. Besides, its divalent oxalate anion ($C_2O_4^{2-}$), it is a good reducing agent. Also, oxalic acid is a bidentate complexing agent that can exist in aqueous solutions in different forms, namely, $H_2C_2O_4$, $HC_2O_4^-$ and $C_2O_4^{2-}$, denoting for brevity, H_2L, HL^- and L^{2-}, respectively. The equilibrium between these three species may be as follows [29]:

$$H_2L \xleftrightarrow{pK_1=1.250} HL^- \xleftrightarrow{pK_2=4.266} L^{2-} \quad (1)$$

On the other hand, hydrogen is considered one of the most promising future fuels for being versatile, efficient and clean [30-32]. The concept of producing hydrogen by the reaction of certain cheap and abundant metals with acids for reduction of capital and operating costs holds a key to facilitate the wide spread use of this technology [33,34]. Assessment of this issue was among our motivations to thoroughly investigate the present electrochemical system. Upon reviewing the literature, we found that few available studies are reported on the electrochemical properties of nickel [24-28] or nickel based materials [5,35] in organic acids. Therefore, the present work is focused on using various techniques to study the electrochemical properties of pure nickel in oxalic acid aqueous solutions of different concentrations and temperatures. Furthermore, the effect of adding various sodium halides or azide salts to the Ni/oxalic acid system is also investigated in order to elucidate any relevant activation or inhibition role on the behavior of our system depending on the specificity of the tested halide.

2. EXPERIMENTAL

The nickel samples used as working electrodes were cut from polycrystalline nickel rod (99.99% purity), Johnson Matthey LIT (England). Each sample was encapsulated into glass tube of appropriate internal diameter and fixed with epoxy resin leaving a front cross-sectional surface of area 0.196 cm^2 to contact the test solution. Prior to each experiment the working electrode was mechanically abraded using successive grades of emery papers: 400, 600, 800, 1000 and 1500 grit, rinsed with acetone and finally with deionized water, dried in air and transferred quickly to the electrolytic cell. Electrochemical measurements were performed in a conventional three-electrode cell furnished with a large Pt sheet (2 cm x 4 cm) counter electrode and saturated calomel (SCE) reference electrode. All potentials were measured and referred to the SCE electrode (E_{SCE} = 0.242 V vs. SHE).

Test solutions were prepared from analytical grade reagents (Aldrich or BDH) and deionized water. Fresh oxalic acid solutions of different concentrations were prepared from concentrated 1.0 M stock solution by appropriate dilution.

Electrochemical impedance spectroscopy (EIS) and DC polarization experiments were performed using the electrochemical workstation Zennium Zahner, Mess system, Germany, controlled by PC and Thales Z1.28 Software. Potentiodynamic polarization measurements were recorded using a scan rate of 1 mV s^{-1} to achieve quasi-stationary conditions. Linear sweep voltammetry scans were also carried out at a rate of 50 mV s^{-1}. The AC impedance response and phase shift (φ) measurements were traced at the open circuit potential (OCP) with 10 mV peak to peak sinusoidal perturbation signal in the frequency domain from 100 kHz down to 0.1 Hz. To achieve reproducibility, each experiment was carried out at least twice. All measurements were always carried out at 25 ± 1 ^{o}C unless otherwise stated, using naturally aerated stagnant solutions. Examination of sample surfaces were carried out using scanning electron microscope (SEM), Quanta FEG250 high field emission system (Japan).

3. RESULTS AND DISCUSSION

3.1. Open circuit potential measurements

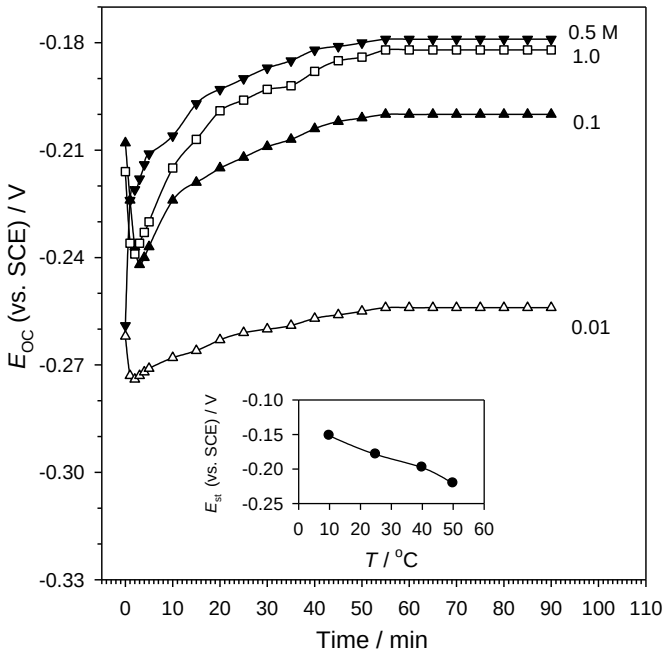

Figure 1. Variation with time of the open-circuit potential (E_{oc}) of Ni electrode in oxalic acid solutions as a function of its concentration at 25 ^{o}C. Inset: variation of the steady state potential (E_{st}) as a function of temperature after 90 min. from Ni electrode immersion.

Fig. 1 shows variation with time of the free OCP (E_{oc}) of Ni electrode in aqueous oxalic acid solutions as a function of concentration over the range 0.01-1.0 M. As can be seen, for the first few

minutes following immersion E_{oc} drifts quickly in the negative direction due to partial dissolution of the native oxide film on the metal surface [36]. After then, the potential inclines in the positive direction and increases gradually until achieving a quasi-steady value (E_{st}) during ~ 45 min. The positive shift in the potential reflects a tendency for oxalic acid solution to passivate nickel, possibly due to growth of a protective film on its surface [36,37]. However, as the proton concentration in solution slightly decreases at the higher oxalic acid concentration 1.0 M) the dynamic equilibrium between passive film dissolution and formation processes is shifted more towards dissolution leading to a small decrease in E_{st} value of nickel electrode.

The effect of temperature over the range 10-50 ^{o}C on the OCP evolution of nickel in 0.5 M oxalic acid solution was also examined. At all tested temperatures the E_{oc} transients exhibit a very similar pattern to one described above. However, raising ambient temperature causes E_{st} value recorded after 1 h immersion to decrease almost linearly (inset Fig. 1). Such behavior may be ascribed to thermal activation of a film thinning process, or growth of a more defective film with lower protective capability on the metal at higher temperature. Both reasons may enhance the corrosion susceptibility of nickel and extent of hydrogen evolution (HE) on its surface with raising temperature [34]. However, the exact explanation for that behavior can be properly gained from EIS data recorded at the steady OCP (E_{st}) as a function of temperature.

3.2. AC impedance measurements

Electrochemical impedance spectroscopy (EIS) is a useful non-destructive technique. It can provide valuable information about the ongoing process such as corrosion, film formation, discharge of batteries or any other electrochemical action. Change in values for the individual components of an equivalent electronic model simulating the EIS data of the surface/electrolyte interface indicates their behavior and performance [38]. Therefore, to confirm the OCP results and get more insights into the electrochemical properties of Ni in oxalic acid solutions and its surface film performance in those electrolytes EIS investigations were done at OCP.

3.2.1. Effect of concentration

Fig. 2 presents the impedance Bode plots of Ni electrode recorded after 1 h immersion in naturally aerated oxalic acid solutions of different concentrations at 25 ^{o}C. The salient features of nickel spectra on the Bode format reveal a single phase peak, which shifts gradually to higher frequency (HF) and higher phase maximum (φ_{max}) with increasing acid concentration up to 0.5 M. After then, φ_{max} decreases slightly and moves toward lower frequency (LF) as the concentration is increased. Besides, the global impedance ($|Z|$) at the LF range shows a wide capacitive response which increases with increasing concentration up to 0.5 M, followed by a slight decrease in its value for concentration > 0.5 M. These data suggest that oxalic acid can enhance the growth of a protective film on nickel surface over the range 0.01-0.5 M. However, further increase in acid concentration leads to a

slight decrease in the protection efficiency of this film likely due to its partial dissolution as the solution pH is re-increased a little.

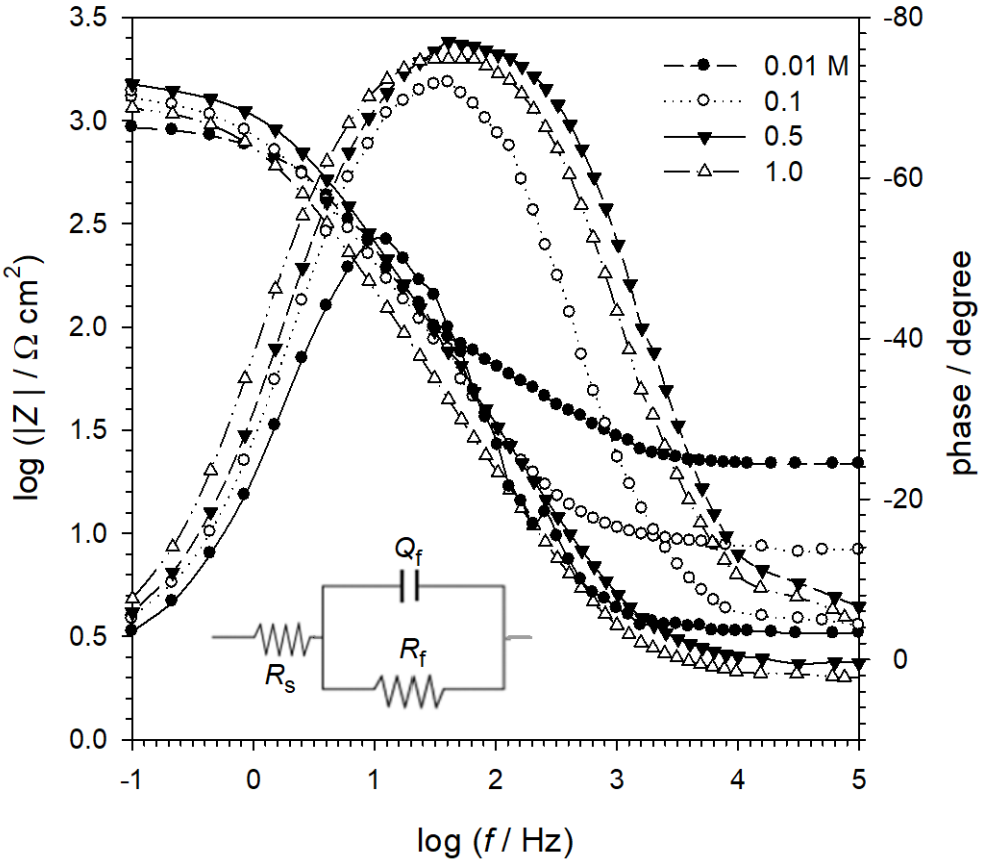

Figure 2. Bode plots for the EIS data of Ni after 90 min. immersion in oxalic acid solutions as a function of concentration at 25 °C, points are measured data and solid lines are the best fitted values. Inset: one-time constant equivalent circuit model used to fit the experimental impedance data.

As there is no evidence for the presence of two or more time constants, the equivalent circuit shown in the inset of Fig. 2 was used for analyzing the measured impedance data for Ni electrode. The circuit model is based on a single parallel combination of the anodic and cathodic responses at OCP. A constant phase element (CPE) is used to replace the pure capacitive element (C) to account for the dispersion effect caused by roughness of the electrode surface [39]. The impedance of the CPE is defined by [40]: $Z_{CPE} = 1/Q(j\omega)^{\alpha}$, where Q is a constant independent of the frequency and having units of F cm^{-2} s$^{\alpha}$. The factor α is the CPE power ($0 \leq \alpha \leq 1$) and its deviation from unity is indication of deviation of Q from ideal capacitance (C), $j = \sqrt{-1}$ and ω is the angular frequency in rad s^{-1} ($\omega = 2\pi f$, f being the frequency of the applied perturbation signal in Hz or s^{-1}). Herein, the CPE is assigned to the protective film on Ni surface and not to the double layer capacitance as confirmed by plotting the logarithm of imaginary part of the impedance response (log Z_{img}) vs. log f as depicted in Fig. 3, where the constant slope with ($-\alpha$) value indicates the presence of the film.

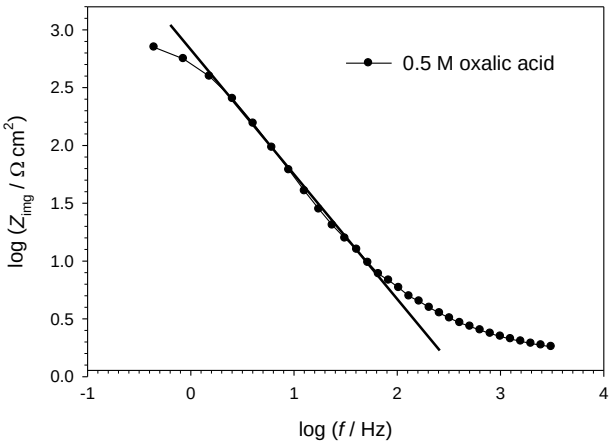

Figure 3. Plot of logarithm imaginary part of impedance (log Z_{img}) as a function of log (*f*) for Ni in 0.5 M oxalic acid.

Table 1. Equivalent circuit parameters of Ni electrode after 90 min immersion in oxalic acid solutions as a function of concentration, temperature and kind of the added 0.1 M NaX halide or azide salt to 0.5 M oxalic acid solution.

[oxalic acid] (M)	R_f (kΩ cm^2)	C_f (μF cm^{-2})	α	R_s (Ω cm^2)	1/ C_f (μF^{-1} cm^2)
0.01	0.67	4.29	0.83	37.4	0.233
0.1	1.02	4.42	0.82	6. 9	0.226
0.5	1.11	4.71	0.89	1.9	0.212
1.0	0.88	7.75	0.88	1.6	0.129
T (K)[a]					
283	1.40	4.85	0.90	2.1	0.206
298	1.11	4.71	0.89	1.9	0.212
313	0.52	3.10	0.89	1.8	0.322
323	0.34	2.93	0.89	1.6	0.342
0.5 M oxalic acid + 0.1 M X$^-$					
I$^-$	4.88	1.48	0.89	2.2	0.675
F$^-$	1.82	3.21	0.89	4.1	0.312
Blank	1.11	4.71	0.89	1.9	0.212
Cl$^-$	1.01	4.56	0.85	2.4	0.219
Br$^-$	0.21	4.06	0.84	1.5	0.246
N_3^-	0.05	2.46	0.66	8.1	0.407

[a] of 0.5 M oxalic acid solution

The above equivalent circuit was found to be quite satisfactory to fit the obtained EIS data with an average error of less than 1.3%. Data simulation and analysis was performed using Thales *Z1.28* software provided with the electrochemical workstation and the mathematical complex formulation of the total impedance for a solution resistance (R_s) connected serially to a parallel network which represents the time constant (R_f Q_f) as given by the following complex function [36,41]:

$$Z(j\omega) = R_s + \frac{1}{1/R_f + (j\omega Q_f)^{\alpha}} \quad (2)$$

where R_f and Q_f indicate the resistive and capacitive behavior of the surface film on metallic Ni [36,41]. The Q value is identical to the pure capacitance at $\omega = 1$ [42,43], then $Q_f = C_f$. Based on that, the equivalent circuit parameters were estimated and compiled in Table 1.

Generally, the film resistance (R_f) increases with oxalic acid concentration over the range 0.01-0.5 M. However, at higher concentration R_f value experiences a small decrease again possibly due to the re-increase in pH value of solution as it was experimentally evident. The pH values of as-prepared tested oxalic acid solutions were measured as equal to: 3.05, 1.51, 1.70 and 2.35 for 0.01, 0.1, 0.5 and 1.0 M, respectively. It is well established that passivity of nickel is intimately related to the pH of the contacting medium [2] and oxalate anion is an excellent bidentate legand in coordination chemistry. It follows herein that the interaction between nickel surface and oxalic acid will be complicated. For the concentration range 0.01-0.5 M, the following stable complexes may be formed with the divalent nickel cation (Ni^{2+}) [44]:

$$Ni^{2+} + H_2L \rightarrow [NiHL]^+ + H^+ \quad (3)$$

$$\text{and/or } Ni^{2+} + H_2L \rightarrow NiL + 2H^+ \quad (4)$$

These complexes can precipitate on the flawed area and weak spots within the surface and help to increase sealing properties of the surface oxide film. On the other hand, at higher oxalic acid concentration (> 0.5 M), a possibility of forming more soluble complex with lower stability constant ($K_{st} = 3.23\times10^{-9}$ [44]) is not excluded according to:

$$Ni^{2+} + H_2L + H_2O \rightarrow [Ni(OH)L]^- + 3H^+ \quad (5)$$

This will cause an instability of the interfacial nickel oxide film and consequently the value of its film resistance (R_f) is going to be slightly decreased.

3.2.2. Effect of temperature

The impedance behavior of Ni in 0.5 M oxalic acid solution was also scrutinized over the temperature range 10-50 ^{o}C. Upon raising the ambient temperature Fig. 4(a) demonstrates a continuous decrease in the absolute impedance, indicating a simultaneous decrease in the surface film stability. An additional evidence for that can be perceived from the increase in the phase angle (φ) and the broadening of φ vs. log f spectra as the solution temperature is lowered, suggesting a decrease in the corrosion vulnerability of nickel [42].

As it can be seen from the estimated parameters listed in Table 1, both R_f and C_f values of the surface film decrease with rise in temperature confirming that thermal energy can promote the corrosion process of nickel in oxalic acid solution with a subsequent increase in the rate and extent of HE on its surface, which can also be clearly observed with the necked eye. Accepting the simple parallel plate model for the interface region, the thickness (L in cm) of the passive film formed on the specimen will be a direct function of its reciprocal capacitance ($1/C_f$ in F^{-1} cm^2) in accordance of the simple expression [45]:

$$L = A\varepsilon_o \varepsilon_r / C_f \quad (6)$$

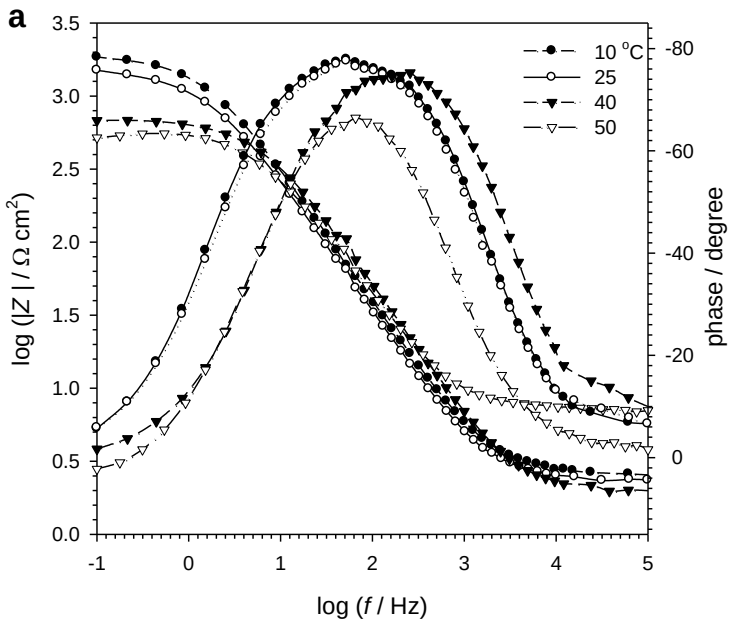

Figure 4(a). Bode plots for EIS data of Ni after 90 min. immersion in 0.5 M oxalic acid solution as a function of temperature.

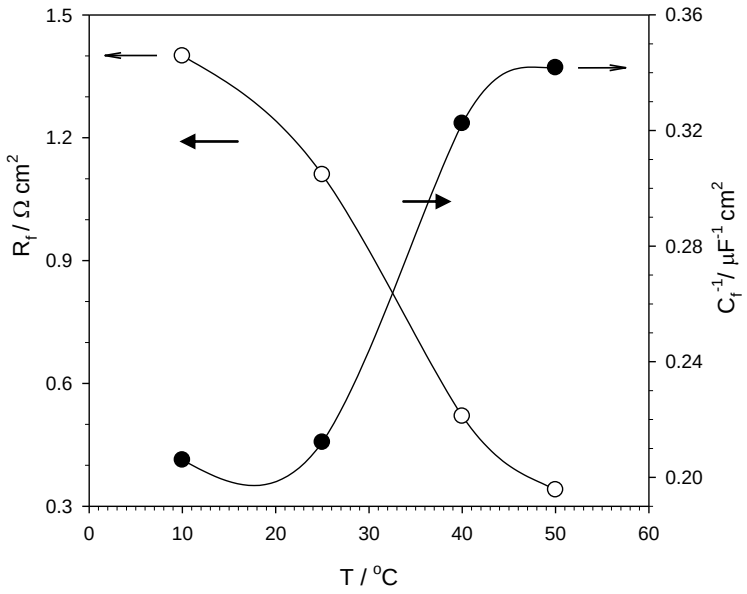

Figure 4(b). The resistance (R_f) and relative thickness ($1/C_f$) of the surface film formed on Ni after 90 min. immersion in 0.5 M oxalic acid solution as a function of temperature.

where A in cm^2 is the electrode area, ε_o is the permittivity of the free space (8.85×10^{-14} F cm^{-1}) and ε_r is the relative dielectric constant of the film. Fig. 4(b) shows the dependence of the surface film resistance and its relative thickness ($1/C_f$) on temperature. The present findings indicate that temperature can sustain the growth of a much thicker and defective film on nickel surface in oxalic acid electrolyte, where its resistance decreases and consequently the film becomes less protective with

raising solution temperature. This may be due to the fact that thermal energy usually enhance chemical and electrochemical reactions in the interface region and create significant modification in the microstructure of the pristine film [34].

3.3. Potentiodynamic Polarization Measurements

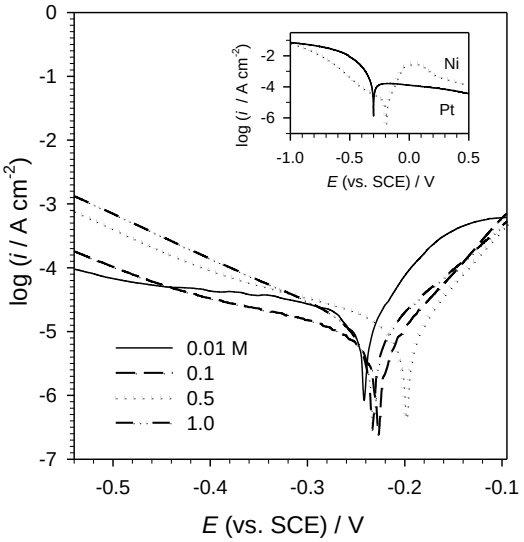

Figure 5. Cathodic and anodic polarization curves of Ni after 90 min. immersion in oxalic acid solutions as a function of the acid concentration at 25 ^{o}C and scan rate 1 mV s^{-1}. Inset: polarization curves of Pt and Ni electrodes in 0.5 M oxalic acid solution.

Fig. 5 shows typical polarization (*E*-log *i*) plots of Ni electrode traced at scan rate of 1 mV s^{-1} after 90 min immersion in oxalic acid solutions with different concentrations at 25 ^{o}C. As may be indicated the anodic Tafel branch attained higher active dissolution current densities at lower acid concentration. On the other hand, the cathodic polarization branch follows also Tafel behavior, assuming to represent the cathodic reduction of the prevailing proton in the present acidic solution:

$$2\,H^{+} + 2\,e^{-} \rightarrow H_2 \uparrow \quad (7)$$

At any given cathodic potential, the current density for hydrogen reduction (i_H) clearly increases with increasing acid concentration or raising solution temperature. This was also associated with a visual excessive evolution of hydrogen bubbles on the working electrode. The polarization curves were exploited to determine the electrochemical corrosion parameters of Ni in oxalic acid solutions as a function of both concentration and temperature, using the software for *i*/*E* analysis [34,36,42,45]. As a matter of fact, only pure charge transfer controlled current can be accepted as true Tafel data [46-48]. Thus, the corrosion current density (i_{corr}) for the corrosion process was estimated by the intersection of the cathodic Tafel line back to the E_{corr} value (i.e. potential of zero current in the potentiodynamic curves), as listed in Table 2.

Table 2. Electrochemical corrosion parameters of Ni electrode after 90 min immersion in oxalic acid solutions as a function of concentration, temperature and kind of the added 0.1 M NaX halide or azide salt to 0.5 M oxalic acid solution.

[oxalic acid] (M)	i_{corr} µA cm^{-2}	E_{corr} / V (vs. SCE)	β_c mV/dec	β_a mV/dec	R_p (kΩ cm^2)	i_o (µA cm^{-2})
0.01	19.8	-0.238	-209	65	1.086	19.2
0.1	8.7	-0.241	-202	64	2.426	12.6
0.5	7.7	-0.242	-171	75	2.940	11.6
1.0	8.2	-0.232	-136	85	2.770	14.6
T(K)[a]						
283	6.2	-0.188	-170	59	3.067	8.7
298	7.7	-0.199	-171	75	2.940	11.6
313	16.9	-0.232	-172	67	1.239	25.9
323	27.5	-0.322	-185	88	0.916	40.9
0.5 M oxalic acid + 0.1 M X$^-$						
I$^-$	1.4	-0.117	-88	46	9.369	2.6
F$^-$	5.1	-0.194	-108	59	3.249	7.1
blank	7.7	-0.199	-171	75	2.940	11.6
Cl$^-$	26.4	-0.292	-100	70	0.677	12.7
Br$^-$	49.1	-0.205	-91	61	0.323	61.1
N_3^-	482.5	-0.109	-86	62	0.033	256.7

[a] of 0.5 M oxalic acid solution (blank)

It is worth to note that the recorded E_{corr} values are somewhat different from the steady state (E_{st}) values shown in Fig. 1, that may be attributed to surface activation and partial removal of the native passive film. This is because polarization scans were started at more negative potential relative to E_{st} [49-51]. The cathodic Tafel slope (β_c) was found to be around 180 mV/decade on the average in good accord with the previously reported value for HE reaction on Ni in acidic media [20]. From Table 2 it is evident that the corrosion rate of the metal in terms of i_{corr} increases upon lowering oxalic acid concentration (over the range 0.01-0.5 M) or raising the solution temperature, indicating a noticeable decrease in the propensity of nickel to seal its surface film under these conditions. This behavior accords well with the EIS results.

Based on the present impedance data, and considering that charge transfer resistance (R_{ct}) value is equivalent to that of film resistance (R_f) in the Randles model used for our data fitting analysis, the exchange current density (i_o) may be evaluated from the following theoretical relation [51]:

$$i_o = RT/nFR_{ct} \quad (8)$$

where R is the gas constant in J mol^{-1} K^{-1}, T is the absolute temperature in K, F is the Faraday constant (96487 C mol^{-1}) and n is the number of electrons exchanged during the nickel dissolution process.

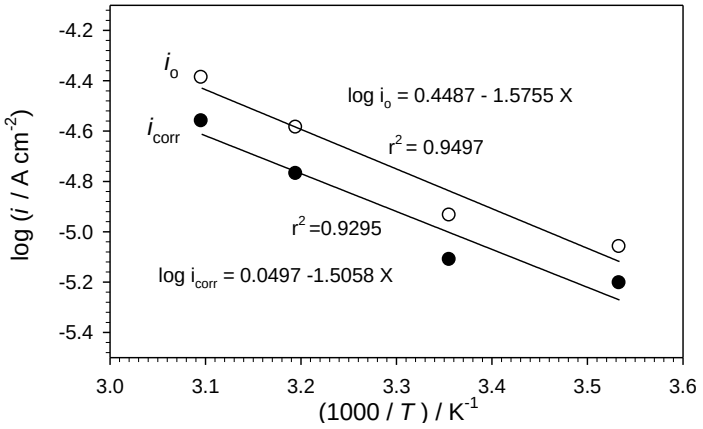

Figure 6. Arrhenius plots of i_{corr} (DC) and i_o (AC) for Ni electrode in 0.5 M oxalic acid solution.

Table 2 and Fig. 6 show that the corrosion (i_{corr}) and exchange (i_o) current densities are both increased linearly with 1/T on a semi-logarithmic plots in accordance with the Arrhenius law [34,36,51,52] as represented in the following equation:

$$\log i = \log A_o - \left(\frac{E_a}{2.303R}\right) \cdot \frac{1}{T} \quad (9)$$

Where A_o is the Arrhenius pre-exponential factor and E_a is the apparent activation energy of the electrochemical process in J mol^{-1}. Eq. (9) offers estimation for the effective activation energy of the corrosion process from the measured DC and AC data. As shown in Fig. 6, the slopes of the two linear plots give values for E_a as 28.8 and 30.0 kJ mol^{-1}, respectively, in agreement with those previously reported for nickel in 1.0 M LiBr [51]. The difference in E_a value obtained by the two different techniques can be explained if considering that at OCP nickel electrode is under its spontaneous passive state. Therefore, the corrosion process kinetics is under anodic control, which essentially differs from the equilibrium dissolution defined by the i_o parameter. Even though, the two values are still more than that for diffusion barrier in aqueous environments which provides an argument in favor of a solid-state diffusion model for Ni metal in oxalic acid solution [34].

3.4. Linear Sweep Voltammetry Measurements

Polarization performance of nickel in oxalic acid solutions was also inspected via linear sweep voltammetry (LSV). Fig. 7 presents typical voltammograms of nickel electrode recorded in the positive going scan at a rate of 50 mV s^{-1} after 90 min immersion as a function of acid concentration. Prior to ~ -0.4 V (vs. SCE) hydrogen gas evolution was observed to be more intensive with increasing negative polarization.

The cathodic current density gradually decreases with the applied potential reaching zero at E_{corr} and stabilizes at this value for a certain potential region. This transition zone may be related to a formation of α-Ni(OH)$_2$ passive layer on the metal [53].

$$Ni^0 + 2OH^- \rightarrow \alpha\text{-}Ni(OH)_2 + 2e \quad (10)$$

In the recent years, namo-nickel hydroxide is considered a promising electrode in supercapacitors [54].

To compare nickel reactivity toward cathodic hydrogen reaction with that of platinum, which is the metal with the highest catalytic activity for the HER, the hydrogen overpotential (η_H) is estimated for both metals at the same oxalic acid concentration.

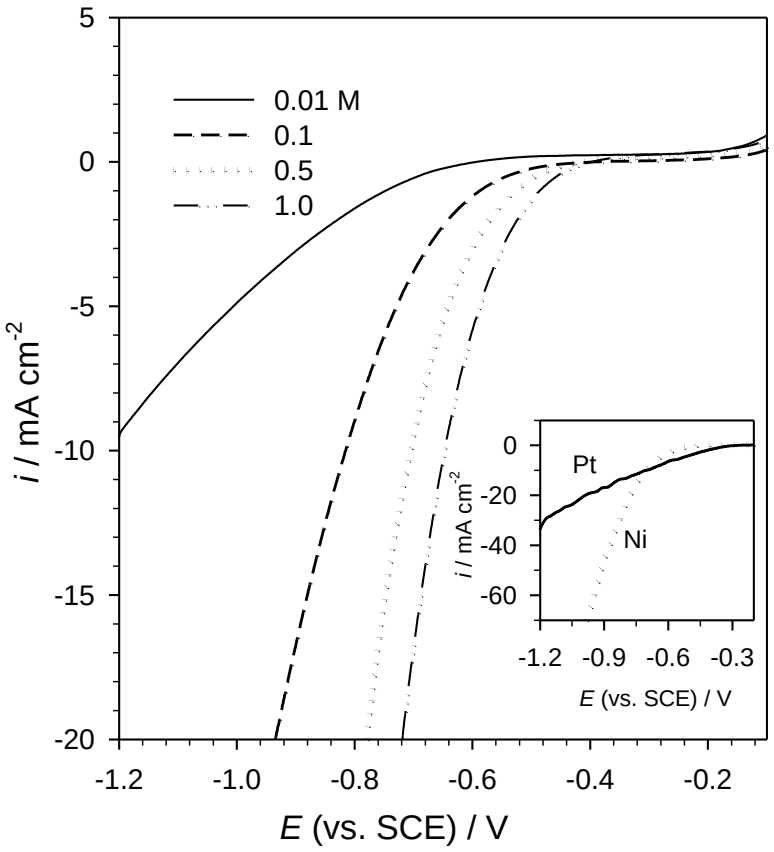

Figure 7. Linear voltammograms of Ni electrode in oxalic acid solutions as a function of oxalic acid concentration at 25 ^{o}C and scan rate 50 mV s^{-1}. Inset: cathodic polarization trace of Pt and Ni electrodes in 0.5 M oxalic acid solution at 25 ^{o}C and scan rate 50 mV s^{-1}.

The steady state potentials (E_{st}) of Ni and Pt are -0.181 V and 0.444 V, respectively, as experimentally measured after 90 min immersion in 0.5 M oxalic acid solution. Also, the potential at which hydrogen starts to evolve in the same solution at Ni is -0.532 V and at Pt is -0.298 V (Fig. 7 inset). Interestingly, the estimated η_H value amounts to -0.351 V on Ni whereas that on Pt is -0.742 V, implying that nickel may be considered a promising cathode for HE in oxalic acid solution. Furthermore, to contrast Ni and Pt from the point of view of HER rate at one and same polarizing potential, it is indicated that nickel is not only comparable but also seems better than Pt. For example, in 0.5 M oxalic acid solution at -1.0 V vs. SCE the current density corresponds to HER on Ni amounts to -72 mA cm^{-2}, whereas its value on Pt amounts to only -20 mA cm^{-2}, indicating a faster HER rate on nickel surface than on platinum.

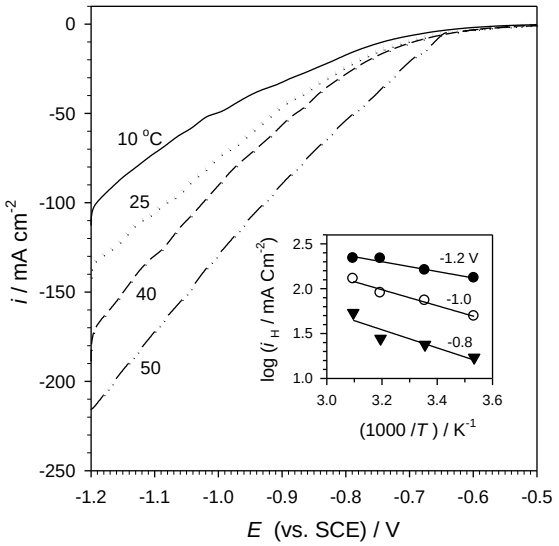

Figure 8. Cathodic polarization trace of Ni electrode in 0.5 M oxalic acid solution as a function of temperature at scan rate 50 mV s^{-1}. Inset: Arrhenius plots of the cathodic hydrogen evolution on Ni electrode in 0.5 M oxalic acid solution at different polarizing potentials of -0.8, -1.0 and -1.2 V (vs. SCE).

Fig. 8 depicts the effect of temperature on the cathodic LSV of Ni surface in 0.5 M oxalic acid solution, demonstrating that the rate of hydrogen evolution increases as temperature is increased. In general, temperature rise favors the kinetics of HER on nickel in oxalic acid but delays its passivation as it enhances the anodic dissolution of the metal via the active sites on the surface. Basically, at any specified cathodic potential the rate of HER is directly proportional to its corresponding cathodic current density (i_c) [51-55]. The Arrhenius plots for i_c values at -0.8, -1.0 and -1.2 V (vs. SCE) are also presented as inset in Fig. 7. The activation energy ($E_{a,H}$) for the HER estimated from the slopes of the linear dependence of log i_c vs. $(1/T)$ according to Eq. (9), was found to decrease with increasing the polarizing cathodic potential. The lower the activation energy is, the lower the energy required for hydrogen evolution at higher cathodic potential. The obtained values are 19.4, 17.1 and 10.5 kJ mol^{-1} at -0.8, -1.0 and -1.2 V vs. SCE, respectively. The low activation energy values for hydrogen production is connected with the ease of its reduction on nickel surface in oxalic acid solution and supports that HER is a single electron transfer process [34,55]. It is generally accepted that HER occurs via two successive steps. The first is the discharge of H_3O^+ cation to give adsorbed hydrogen atom (H_{ad}), and the second step is dimerization of adsorbed hydrogen atom [52,55]. Either step or both can be the rate determining step depending on crystallographic orientation of the electrode surface and its type [56,57].

3.5. Effect of halide ion addition

This section is devoted to clarify the peculiar influence of various halides and azide nature on the electrochemical performance of Ni in oxalic acid solutions, depending on the specificity of each

ion. Fig. 9 presents EIS of Ni electrode conducted after 1h immersion in 0.5 M oxalic acid solution free or containing 0.1 M sodium salt of either fluoride, chloride, bromide, iodide or azide. The pH values of these solutions as measured are, respectively: 1.28, 1.13, 1.10, 1.03 and 1.33. The results demonstrate that the impedance modulus ($|Z|$) at the LF range and the phase maximum (φ_{max}) in the MF range are both increased in the following sequence: $I^- > F^- >$ free acid $> Cl^- > Br^- > N_3^-$ (the least). All spectra were fitted to the above equivalent circuit (shown in Fig. 2 inset), and the estimated simulated circuit parameters are compiled in Table 1 as a function of the identity of the added anion.

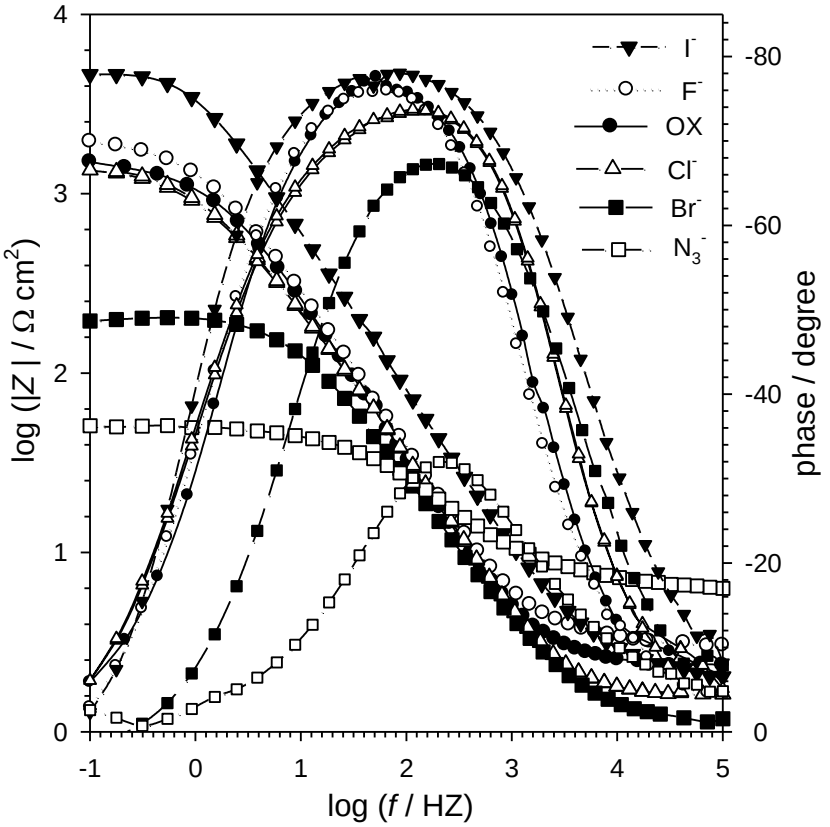

Figure 9. Bode plots for EIS data of Ni after 90 min. immersion in naturally aerated 0.5 M oxalic acid solution free or containing 0.1 M NaX (halide) or NaN_3 (azide) salt at 25 ^oC.

The electrochemical corrosion of Ni/oxalic acid system in the presence of various anions was also studied by recording potentiodynamic polarization curves of Ni in 0.5 M oxalic acid solutions free or containing 0.1 M NaX salt (not shown). Compared with the behavior in the free acid, the polarizing current density was found to be much lower in presence of I^- ions and much higher in presence of N_3^- ions in good accord with the EIS results. Basically, the polarization curves were mainly used to estimate all electrochemical corrosion parameters of Ni as a function of X^- anion type as given in Table 2. The results show a significant increase in the value of the corrosion current density on going from solution containing I^- ions (i_{corr} = 1.4 μA cm^{-2}) to the other including N_3^- ions (i_{corr} = 482.5 μA cm^{-2}) following the order: $I^- < F^-$ < free acid < $Cl^- < Br^- < N_3^-$ (the most aggressive) which mirror completely the rank for decreasing R_f value (see Table 1).

Table 3. Values of the halide ionic radius (*r*), the hydrated (*r*), the surface charge density (σ), the hydration enthalpy (ΔH_h) and the viscosity B-coefficient at 25^oC, of the studied anions [59].

Anion	*r* (nm)	Hydrated *r* (nm)	σ (mC m^{-2})	ΔH_h (kJ mol^{-1})	*B* (L mol^{-1})
F^-	0.133	0.212	720.16	-510	0.10
Cl^-	0.181	0.224	388.84	-367	-0.007
Br^-	0.196	0.231	331.60	-336	-0.032
I^-	0.220	0.246	263.20	-291	-0.068
N_3^-	0.850[1]	-	17.63[2]	-	-0.021[58]

[1] M.-L. Brouty, C. R. Acd. Sc. Paris, 214 (1942) 480.
[2] Calculated using the relation: $\sigma = ze/4\pi r^2$, where e = 1.6x10^{-19} C and z is the ion valency.

Interpretation of most of these results can be ascribed to the kosmotrope/chaotrope nature of the added ions which is related to their ability to highly/poorly structure the water molecules in their vicinity. It is known that azide ion is commonly regarded as a pseudo-halide anion [58]. Referring to the data in Table 3, the investigated anions encompass small ions with a relatively high surface charge density (σ), that generate high electric fields at short distance, and referred as water-structure making ions, named kosmotrope (like F^-). The others presenting the opposite effect which are water-structure breaking ions, named chaotropes. Those are relatively large, generating a relatively weak surface charge density, thus prone to lose their hydration shell. Consequently, the influence of our tested ionic additives may be conveniently distinguished according to the sign of the viscosity B-coefficient appearing in the well- known Jones-Dole empirical relationship [58]. This B-coefficient is a direct measure of the strength of the ion-water interaction, where B > 0 for kosmotrope ions, while B < 0 for chaotrope ones. Therefore, in light of the present results and following Table 3, the chaotrope anions Cl^-, Br^- and N_3^- can easily act as corrosion accelerators for nickel metal decreasing the stability of its passive film and simultaneously enhance HE reaction at its surface. For this group, the anion aggressiveness towards active dissolution of nickel in oxalic acid increases in the order: $Cl^- < Br^- < N_3^-$ (highest). This is the same sequence of increasing their ionic radii and decreasing their energies of hydration [45,60], i.e. increasing their tendency for adsorption on the metallic substrate. They may then be able to penetrate into the passive layer and involved in a thinning process through the formation of soluble salts or complexes with surface metallic cations (Ni^{2+}), and thus inhibiting nickel passivation [53,61].

However, nickel passivity increases by the presence of iodide ions despite its chaotrope nature (B < 0) where the obtained i_{corr} value decreases to 1.4 μA cm^{-2} and R_f value increases to 4.88 kΩ cm^2 that's relative to their values in the free acid solution as being 7.7 μA cm^{-2} and 1.11 kΩ cm^2, respectively. The distinction in the behavior of iodide in oxalic acid media is likely attributed to the propensity of the ions to form more stable complexes with surface nickel cations. These findings coincide with the previously reported results pointing out that KI addition to sulfuric acid medium exhibited inhibition of the anodic nickel corrosion process and decreased the corrosion rate of the metal without changing the mechanism [62]. The efficacy of inhibition by iodide ion is likely attributed to its higher adsorbability on the oxide-free metallic area forming a negatively charged

surface. Hydrogen positive ion compensates the negative charge changing the structure of double layer. This can lead to passivation of active locations and consequently assists to preclude electrochemical corrosion of nickel in oxalic acid medium.

On the other hand, for fluoride ions having kosmotrope character (B > 0) the hydration shell around the ions is thick and held strongly. Hence, the impact of fluoride on nickel performance in oxalic acid solution is different from the others (*i.e*. chloride, bromide and azide), where corrosion is prevented and passivity is enhanced, possibly due to preserving the oxide film on the substrate and the formation of insoluble fluoride salts on its surface [63]. This also accords with the fact that nickel is one of the few metals which can be used to store or transport hydrogen fluoride (HF) or elemental fluorine (F_2), as the formed passive film can perfectly coat the nickel surface [64]. Generally, the obtained results indicate different propensities for the investigated anions to enhance the sealing and barrier properties of the surface film on nickel in oxalic acid medium *via* a coupled dissolution-formation mechanism.

Evidence in favor of the above mentioned behavior can be validated from LSV scans in the potential range for HER at Ni electrode in 0.5 M oxalic acid solution free or containing various anions (Fig. 10).

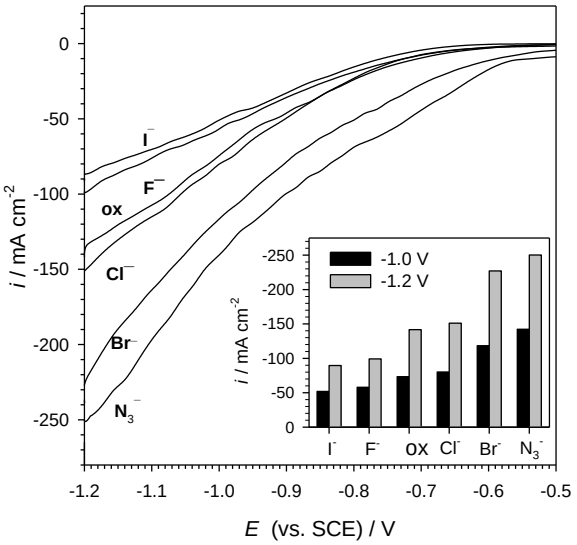

Figure 10. Cathodic polarization trace for Ni electrode in 0.5 M oxalic acid solution free or containing 0.1 M NaX (halide) or NaN_3 (azide) salt at 25 ^oC.

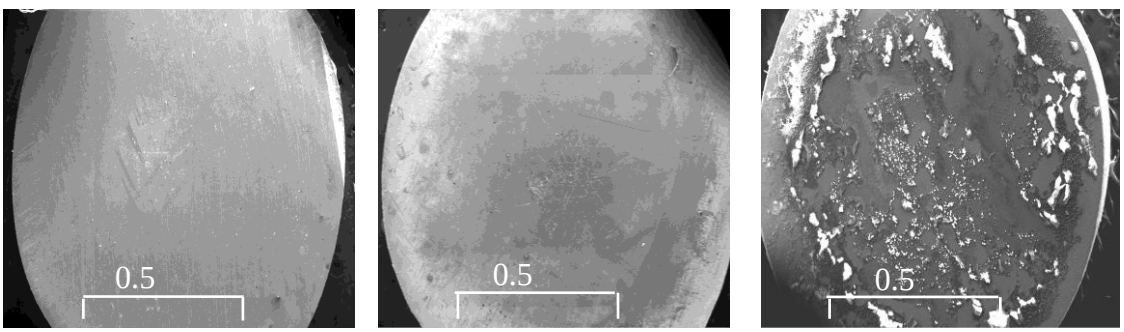

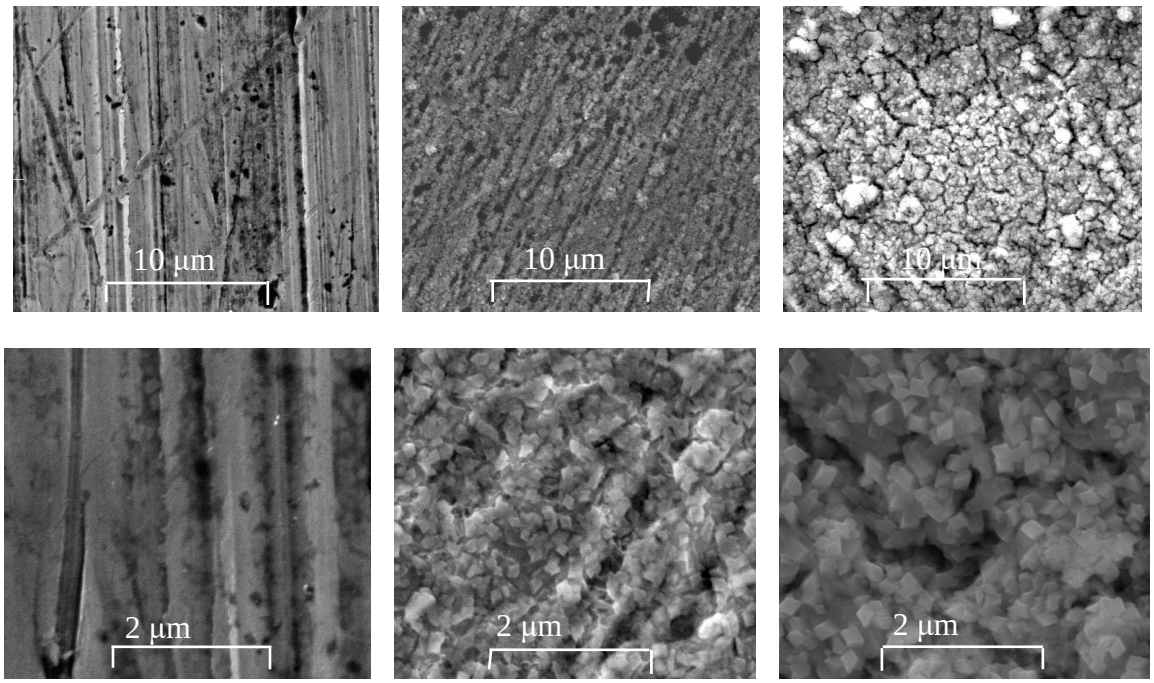

Figure 11. FE-SEM micrographs at different magnifications of nickel samples immersed for 150 min. in 0.5 M oxalic acid solution free or containing 0.1 M iodide or azide ions: (a) with iodide, (b) free acid and (c) with azide.

For any selected cathodic overpotential, the rate of HER (i_c) relative to the value in the free oxalic acid solution increases by a similar order as that for i_{corr} value when oxalic acid solution contains chloride, bromide or azide ions and decreases in presence of iodide or fluoride ions, being the least with iodide (Fig. 10 inset). This implies that among the tested ions, azide proves to be the most aggressive one, whilst iodide is an efficient inhibitor for the nickel dissolution process in oxalic acid. This finding is further supported by SEM examination at various magnifications for three nickel samples a, b and c exposed 150 min to iodide-containing, free-acid and azide-containing 0.5 M oxalic acid solutions, respectively as presented in Fig. 11. It is clear from the surface morphology of the three samples at the lowest magnification that sample (a) is characterized by a bright coherent surface with no trace for corrosion as compared to sample (b) which exhibits a mild corrosion attack. By contrast, the corrosion pattern for sample (c) indicates vulnerable surface dominated by sever dark pits and cracks. Indeed, at higher magnification the images reveal that sample (a) is being intact as it is smeared with a continuous protective layer, which gives an improved surface morphology. On the other hand, the corrosion products layer on sample (b) is mostly closely packed while that on sample (c) is loosely adhered to the sample surface. These prominent variations in the microstructures of the three films reflect the same aptitude for their electrochemical performance as it is effectively observed.

4. CONCLUSIONS

1- Various electrochemical techniques has been used to thoroughly investigate the electrochemical performance of polycrystalline nickel in oxalic acid solutions of different concentrations and temperatures.

2- Over the concentration range (0.01-0.5M) and at all temperatures studied, OCP transients of Ni electrode showed that oxalic acid can sustain the growth of surface film with better performance on Ni metal.

3- EIS data revealed that the surface film resistance (R_f) increases while its relative thickness ($1/C_f$) slightly decreases with increasing concentration. This assumes that oxalate anion as complexing bidendate legand can enhance formation of compact film with better protection ability on metallic nickel. However, raising ambient temperature leads to decrease R_f and increase $1/C_f$ values indicating the growth of a thicker film with more defective nature as the temperature is increased, likely due to thermal activation of the corrosion process. In addition, there is a good agreement between the apparent activation energies of the corrosion process as estimated from DC and AC data, which are found to be equal to 28.8 and 30.0 kJ mol^{-1}, respectively.

4- Addition of 0.1 M from various halides or azide ions to 0.5 M oxalic acid solution modifies the surface film resistance on nickel such that its corrosion rate becomes more serious in the following order: $I^- < F^-$ < free acid < $Cl^- < Br^- < N_3^-$ (the most aggressive). This displays evidence that azide anion which behaves like the other chaotropic halides can significantly enhance hydrogen evolution at nickel surface in oxalic acid solution. In contrast, iodide anion despite its chaotropic nature exhibits good sealing properties for the surface film through adsorption on the oxide-free active locations leading to increase its barrier properties, therefore preventing Ni metal from dissolution in oxalic acid medium. The results were further validated by FE-SEM micrographs.

ACKNOWLEDGMENT
The authors acknowledge the facilities provided by Faculty of Science, Cairo University which helped us with the electrochemical data collection.

References

1. S. Trasatti, , in *Advances in Electrochemical Science and Engineering*, H. Gerscher, C. W. Tobias (Eds), VCH, Weinheim (1992) p. 1.
2. M. Pourbaix, *Atlas of electrochemical equilibria in aqueous solutions*, 2nd ed, NACE, Texas, USA (1974) p. 333.
3. A. I. Muñoz, J. G. Antón, J. L. Guiñón, V. P. Herranz, *Corros. Sci*., 48 (2006) 3349.
4. Q. Q. Liao, Z. W. Y. Yue, J. Li, H. H. Ge, *Corrosion,* 66 (2010) 125002.
5. S. D. Day, M. T. Whalen, K. J. King, G. A. Hust, I. L. Wong, J. C. Estill, R. B. Rebak, *Corrosion*, 60 (2004) 804.
6. E. Sikora, D. D. Macdonald, *Electrochim. Acta*, 48 (2002) 69.
7. P. A. Selembo, M. D. Merrill, B. E. Logan, *J. Power Sources*, 190 (2009) 271.
8. D. D. Macdonald, From *Water Chemistry of Nuclear Reactor Systems 2*, British Nuclear Energy Society; *London; 2nd* International conference on *water chemistry* of *nuclear reactor systems*, London (1981) pp. 229-234.
9. L. L. Wong, D. V. Fix, J. C. Estill, R. D. McCright and R. B. Rebak, *Characterization of the Corrosion Behavior of Alloy 22 after Five Years Immersion in Multi-ionic Solutions*, *Scientific Basis for Nuclear Waste Management XXVI*, Warrendale, PA, Material Research Society (2003) Vol. 757, p.735.

10. D. C. Agarwal, *Nickel and Nickel alloys, in Uhlig's Corrosion Handbook*, 2nd ed, R. W. Revie (Ed), Wiley, New York, USA (2000) p. 831.
11. G. Cordeiro, O. R. Mattos, O. E. Barcia, L. Beaunier, C. Deslouis, B. Tribollet, *J. Appl. Electrochem.*, 26 (1996) 1083.
12. M. R. Barbosa, J. A. Bastos, J. J. Garciá Jareño, F. Vicente, Electrochim. Acta, 44 (1998) 957.
13. F. Sun, G. Meng, T. Zhang, Y. Shao, F. Wang, C. Dong, X. Li, *Electrochim. Acta*, 54 (2009) 1578.
14. A. Seyeux, V. Maurice, L. H. Klein, P. Marcus, *Electrochim. Acta*, 54 (2008) 540.
15. B. MacDougall, M. Cohen, *J. Electrochem. Soc.* 123 (1976) 191.
16. A. Jouanneau, M. Keddan, M. C. Petit, *Electrochim. Acta*, 21 (1976) 287.
17. T. Dickinson, A. F. Povey, P. M. A. Sherwood, *J. Chem. Soc. Faraday Trans*., 73 (1977) 327.
18. J. R. Viche, A. J. Arvia, *Corros. Sci.*, 18 (1978) 441.
19. S. G. Real, M. R. Barbosa, J. R. Viche, A. J. Arvia, *J. Electrochem. Soc*., 137 (1990) 1696.
20. J. Tamm, L. Tamm, J. Arol'd, *Russ. J. Electrochem*., 40 (2004) 1152.
21. O. M. Magnussen, J. Scherer, B. M. Ocko, R. J. Behm, *J. Phys. Chem.* B, 104 (2000) 1222.
22. J. Scherer, B. M. Ocko, O. M. Magnussen, *Electrochim. Acta*, 48 (2003) 1169.
23. V. P. Grigorev, V. M. Kravchenko, I. M. Gershanova, *Protect. Met*., 40 **(**2004) 214.
24. R. N. Singh, V.B. Singh, *Corrosion*, 49 (1993) 569.
25. G. E. Badea, A. Cojocaru, T. Badea, *Rev, Roum, Chim*., 50 (2005) 141.
26. G. E. Badea, T. Badea, *Rev. Roum. Chim*., 50 (2005) 671.
27. H. Radhakrishnan, A. G. Carcea, R. C. Newman, *Corros. Sci*., 47 (2005) 3234.
28. G. E. Badea, T. Badea, *Rev. Roum. Chim*., 53 (2008) 291.
29. S. Aksu, *J. Electrochem. Soc.*, 152 (2005) G938.
30. T. N. Veziroglu, F. Barbir, *Int. J. Hydrogen energy*, 17 (1992) 391.
31. M. Momirlana, T. N. Veziroglu, *Int. J. Hydrogen Energy*, 30 (2005) 795.
32. J. A. Turner, *Science*, 305 (2004) 972.
33. A. A. El-Meligi, N. Ismail, *Int. J. Hydrogen Energy*, 34 (2009) 91.
34. F. El-Taib Heakal, N. S. Tantawy, O. S. Shehata, *Int. J. Hydrogen energy*, 37 19219 (2012)
35. H. Alves, S. Friedrich, H. Werner, J. Klöwer, C. Collet, *Corrosion behavior of nickel alloys in organic acids*, Matériaux (2002) pp. 1-5.
36. F. El-Taib Heakal, A. M. Fekry, M. Z. Fatayerji, *Electrochim. Acta*, 54 (2009) 1545.
37. J. van Drunen, A. F. B. Barbosa, G. Tremiliosi-Filho, *Electrocatalysis*, 6 (2015) 481.
38. A. Lasia, *Electrochemical impedance spectroscopy and its applications*, Springer (2013).
39. A. J. Bard, G. Inzelt and F. Scholz, *Electrochemical dictionary*, 1st ed, Springer, Berlin (2008).
40. G. J. Brug, A. L. G. van den Eeden, M. Sluyters-Rehbach, J. H. Sluyters, *J. Electroanal. Chem*. 176 (1984) 275.
41. K. Jüttner, *Electrochim. Acta* 35 (1990) 1501.
42. F. El-Taib Heakal, Kh. A. Awad, *Int. J. Electrochem. Sci.*, 6 (2011) 6483.
43. D. Marijan, M. Gojic, *J. Appl. Electrochem*., 32 (2002) 1341.
44. J. Peñuela, J. D. Martínez, M. L. Araujo, F. Brito, G. Lubes, M. Rodríguez, V. Lubes, *J. Coord. Chem.* 64 (2011) 2698.
45. F. El-Taib Heakal, A. A. Ghoneim, A. S. Mogoda, Kh. A. Awad, *Corros. Sci*., 53 (2011) 2728.
46. G. T. Burstein, *Corros. Sci*., 47 (2005) 2858.
47. G. Kear, F. C. Walsh, *Corros. Mater*., 30 (2005) S-1.
48. F. El-Taib Heakal, A. M. Fekry, M. Abd El-Barr Jibril, *Corros. Sci.*, 53 (2011) 1174.
49. G. D. Sulka, P. Jozwik, *Intermetallics*, 19 (2011) 974.
50. F. El-Taib Heakal, A. M. Fekry, M. Z. Fatayerji, *J. Appl. Electrochem*., 39 (2009) 583.
51. V. Guiñón-Pina, A. Igual-Muñoz, J. García-Antón, *Corros. Sci*., 51 (2009) 2406.
52. C. González-Buch, I. Herraiz-Cardoma, E. Ortega, J. García-Antón, V. Pėrez-Herranz, *J. Appl. Electrochem*., 46 (2016) 791.
53. J. L. Trompette, L. Massot, H. Vergnes, *Corros. Sci*., 74 (2013) 187.

54. H. B. Li, M. H. Yu, F. X. Wang, P. Liu, Y. Liang, J. Xiao, C. X. Wang, Y. X. Tong, G. W. Yang, *Nat Commun*., 21 May (2013), DOI: 10.1038/ncomms2932.
55. M. A. Domínguez-Crespo, E. Ramírez-Meneses, A. M. Torres-Huerta, V. Garibay-Febles, K. Philippot, *Int. J. Hydrogen Energy*, 37 (2012) 4798.
56. S. A. S. Machado, L.A. Avaca, *Electrochim. Acta*, 39 (1994) 1385.
57. P. H. Riger, *Electrochemistry*, Prentice-Hall, Englewood Cliffs, London, UK (1987).
58. H. D. B. Jenkins, Y. Marcus, *J. Solution Chem*., 22 (1993) 95.
59. G. Jones, M. Dole, *J. Am. Chem. Soc*., 5 (1929) 2950.
60. J. L. Trompette, L. Arurault, S. Fontorbes, L. Massot, *Electrochim. Acta*, 55 (2010) 2901.
61. J. L. Trompette, *Corros. Sci*., 82 (2014) 108.
62. F. Said, N. Souissi, A. Dermaj, N. Hajjaji, E. Triki, A. Srhiri, *Mater. Corros*., 56 (2005) 619.
63. M. G. Fontana. Corrosion engineering. 3rd ed. McGraw-Hill, New York, USA (1986) p. 353.
64. http://en.wikipedia.org/wiki/Nickel(II)_fluoride